Redox-Induced Formation and Cleavage of O−O σ and π Bonds in a Peroxo-Bridged Manganese Dimer: A Density Functional Study

John E. McGrady*

Department of Chemistry, The University of York, Heslington, York, YO10 5DD, United Kingdom

Robert Stranger

Department of Chemistry, The Faculties, The Australian National University, Canberra, ACT 0200, Australia

Received October 26, 1998

The structural and electronic consequences of reduction and oxidation of a peroxo-bridged $Mn_2^{IV/IV}$ dimer, $Mn_2(\mu\text{-}O)_2(\mu\text{-}O_2)(NH_3)_6^{2+}$, are examined using approximate density functional theory. In both cases, the initial electron-transfer step is localized on the metal centers, but subsequent structural rearrangement results in transfer of the excess charge to the μ-O_2 unit, with concomitant regeneration of the $Mn_2^{IV/IV}$ core. Two-electron reduction results in population of the O−O σ* orbital and complete cleavage of the O−O bond, whereas two-electron oxidation depopulates the O−O π* orbital, forming molecular oxygen. The coupling between the metal centers (antiferromagnetic or ferromagnetic) affects the stability of the intermediate species, in which the redox process is metal based, and hence influences the kinetic barrier to bond formation or cleavage. Reductive cleavage of the O−O σ bond is favored when the metal centers are antiferromagnetically coupled, whereas oxidative formation of the π component of the O−O bond is favored by ferromagnetic coupling. The possible implications for the relationship between structure and function in the oxygen-evolving complex found in photosynthetic organisms are discussed.

Introduction

The multiple oxidation states available to transition metal ions make them ideally suited for a role in redox catalysis, linking ligand-based bond formation or cleavage to electron transfer to or from an external source. As a result, clusters of transition metal ions are found at the active sites of numerous electron-transfer enzymes,[1] notably the tetramanganese cluster in the oxygen evolving complex (OEC)[2] (Figure 1), the site of water oxidation in photosynthetic organisms. The biological importance of iron−sulfur clusters[3] is also well established, for example in the enzyme nitrogenase,[4] and dimanganese (catalase),[5] diiron (methane monooxygenase, ribonucleotide reductase),[6] and dicopper (tyrosinase)[7] active sites are also common.

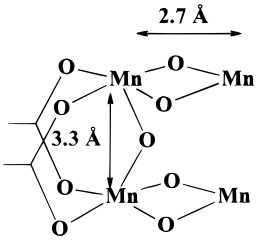

Oxygen-Evolving Complex

$$2H_2O \rightarrow O_2 + 4H^+ + 4e^-$$

Figure 1. Dimer-of-dimers model of the oxygen-evolving complex (OEC) (after Klein et al., ref 2a).

The presence of more than one metal ion in these systems may simply reflect the need to provide multiple oxidizing or reducing equivalents, but it is also possible that interactions between the metal centers play a significant part in overcoming the large kinetic barriers associated with the activation of small molecules.[8] The fact that metalloenzymes operate in aqueous solution at ambient temperatures and pressures is testament to their catalytic efficiency. Clearly an understanding of the structural and electronic basis of their functionality is an important goal, both in its own right, and also because of possible implications for the rational design of industrial

* Address correspondence to this author. Tel.: +44 (0)1904 434 539. Fax: +44 (0)1904 432 516. E-mail: jem15@york.ac.uk.

(1) Holm, R. H.; Kennepohl, P.; Solomon, E. I. *Chem. Rev.* **1996**, *96*, 2239.
(2) (a) Yachandra, V. K.; Sauer, K.; Klein, M. P. *Chem. Rev.* **1996**, *96*, 2927. (b) Pecoraro, V. L.; Baldwin, M. J.; Gelasco, A. *Chem. Rev.* **1994**, *94*, 807. (c) Wieghardt, K. *Angew. Chem., Int. Ed. Engl*. **1989**, *28*, 1153. (d) Rüttinger, W.; Dismukes, G. C. *Chem. Rev.* **1997**, *97*, 1.
(3) Cammack, R., Ed. *Iron−Sulphur Proteins*; Advances in Inorganic Chemistry 38; Academic Press: New York, 1992.
(4) (a) Howard, J. B.; Rees, D. C. *Chem. Rev.* **1996**, *96*, 2965. (b) Kim, J.; Rees, D. C. *Science* **1992**, *257*, 1677. (c) Kim, J.; Rees, D. C. *Nature* **1992**, *360*, 553.
(5) (a) Que, L., Jr.; True, A. E. *Prog. Inorg. Chem.* **1990**, *38*, 97. (b) Dismukes, G. C. *Chem. Rev.* **1996**, *96*, 2909. (c) Fronko, R. M.; Penner-Hahn, J. E.; Bender, C. J. *J. Am. Chem. Soc.* **1988**, *110*, 7554. (d) Beyer, W. F., Jr.; Fridovich, I. *Biochemistry* **1985**, *24*, 6460.
(6) (a) Rosenzweig, A. C.; Frederick, C. A.; Lippard, S. J.; Nordlund, P. *Nature* **1993**, *366*, 537. (b) Rosenzweig, A. C.; Lippard, S. J. *Acc. Chem. Res*. **1994**, *27*, 229.
(7) (a) Magnus, K. A.; Hazes, B.; Thon-That, H.; Bonaventura, G.; Bonaventura, J.; Hol, W. G. J. *Proteins* **1994**, *19*, 302. (b) Volbeda, A.; Hol, W. G. J. *J. Mol. Biol*. **1989**, *209*, 249.
(8) Valentine, A. M.; Lippard, S. J. *J. Chem. Soc., Dalton Trans*. **1997**, 3925.

10.1021/ic981253k CCC: $18.00
Published on Web 01/20/1999

catalysts. In this paper we examine the electronic pathways involved in the formation and cleavage of bonds between oxygen atoms coordinated to a dimanganese cluster, with particular emphasis on how these processes are coupled to the redox chemistry of the cluster. The choice of system leads to obvious comparisons with the chemistry of the OEC, but the purpose of this paper is not to attempt to delineate a complete mechanistic pathway for the evolution of oxygen from water. In our opinion, the structure of the active site is not known with sufficient accuracy to justify this. Instead, we aim to address the more general question of "chemical competence",[8] that is the ability of a particular complex to catalyze a specific chemical transformation. As such, the conclusions drawn are applicable to the general field of redox catalysis, and not just the specific example of the chemistry of the OEC.

The oxidation of water at the OEC is often discussed in terms of the Kok S-state model,[9] wherein four electrons are abstracted from the tetranuclear manganese cluster, inducing release of a molecule of oxygen and regeneration of the reduced cluster. However, structural information on the OEC is available only from indirect sources such as X-ray absorption spectroscopy[10] and electron paramagnetic resonance (EPR),[11] and as a result, the arrangement of atoms within the cluster remains a topic of some debate.[2] Extended X-ray absorption fine structure spectroscopy (EXAFS) indicates that there are two Mn−Mn separations of approximately 2.7 Å,[10a] characteristic of di-μ-oxo bridged manganese systems, and one of 3.3 Å,[10b] typical of a single μ-oxo bridge.[2c] On this basis the dimer-of-dimers structure[10c] illustrated in Figure 1 was proposed as a model for the OEC. The question of the oxidation states of the manganese centers has been addressed using X-ray absorption near edge spectroscopy (XANES) of the manganese K edge, which suggests that, in the S_2 state, a $Mn^{III}Mn_3^{IV}$ cluster is present.[10d−f] Further two-electron oxidation would then result in a formal $Mn_3^{IV}Mn^{V}$ state prior to release of O_2. EPR studies of the S_2 state are consistent with both EXAFS and XANES data,[11] showing a multiline signal very similar to those reported for model systems containing a binuclear $Mn^{III}(\mu\text{-}O)_2Mn^{IV}$ core.[12]

Despite the apparent simplicity of the Kok model, much of the mechanistic detail remains unclear, and numerous proposals regarding the site of water oxidation have been made.[2,10c,13] In such circumstances, where experimental data are limited, theoretical analysis of the fundamental steps of the reaction has an important part to play in establishing the viability of electronic pathways linking reactants and products. Starting from coordinated water or one of its deprotonated forms, OH^- or O^{2-}, the qualitative features of the oxidation process are well established.[14a] A contraction of the O−O vector causes first the O−O σ* and then π* orbitals to rise above the metal manifold (Scheme 1), leading to electron transfer from the antibonding orbitals of the O_2 unit to the metal, forming first peroxide (O_2^{2-}) and then dioxygen O_2. An important feature of Scheme 1 is the correlation of orbitals between the bonded and nonbonded limits, because only if vacant orbitals of the same symmetry as O−O σ* and π* are present in the metal manifold can oxygen be formed in its ground state. However, metal ions in biological systems generally have highly asymmetric coordination environments, and it is not obvious that arguments based on the strict point symmetry of any model system will be relevant to the situation in vivo. There is a more fundamental aspect of the electron-transfer process, however, which is independent of the symmetry of the molecule − the relative orientations of the electron spin. The dioxo $(O^{2-})_2$ and peroxo (O_2^{2-}) oxidation states of the $\{O_2\}$ unit are spin singlets, whereas the ground state of molecular oxygen is a triplet. Consequently the first two-electron oxidation step must involve the loss of two electrons *of opposite spin* from the O−O σ* orbital, but further oxidation to O_2 requires the removal of two electrons *of the same spin* from the orthogonal components of the O−O π* orbital.[15] As we will illustrate, this fundamental difference between the first and second two-electron oxidation processes has significant implications for the electronic structure of the underlying metal cluster.

Scheme 1. Schematic Walsh Diagram Showing the Variation in Energy of σ* and π* Orbitals of the O_2 Unit as the O−O Separation Is Increased

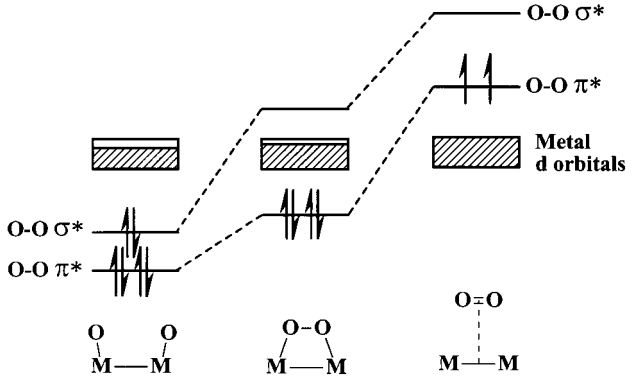

While the electronic principles outlined in the previous paragraph are conceptually simple, the large size and low symmetry of the various models for the OEC has hindered attempts to analyze possible pathways within a computational framework. As a result the majority of work on this and other bioinorganic systems has been performed using extended Hückel theory.[14] More recently, improvements in computational resources have permitted quantitative studies (principally using approximate density functional theory) of the relationship between structure and function in metalloenzyme systems such as methane monooxygenase,[16] nitrogenase[17] and xanthine oxi-

(9) Kok, B.; Forbush, B.; McGloin, M. *Photochem. Photobiol*. **1970**, *11*, 457.

(10) (a) Kirby, J. A.; Robertson, A. S.; Smith, J. P.; Cooper, S. R.; Klein, M. P. *J. Am. Chem. Soc*. **1981**, *103*, 5529. (b) DeRose, V. J.; Mukerji, I.; Latimer, M. J.; Yachandra, V. K.; Sauer, K.; Klein, M. P. *J. Am. Chem. Soc*. **1994**, *116*, 5239. (c) Yachandra, Y. K.; DeRose, V. J.; Latimer, M. J.; Mukerji, I.; Sauer, K.; Klein, M. P. *Science* **1993**, *260*, 675. (d) Roelofs, T. A.; Liang, W.; Latimer, M. J.; Cinco, R. M.; Rompel, A.; Andrews, J. C.; Sauer, K.; Yachandra, V. K.; Klein, M. P. *Proc. Natl. Acad. Sci. U.S.A*. **1996**, *93*, 3335. (e) Ono, T. J.; Noguchi, T.; Inoue, Y.; Kusunoki, M.; Matsushita, T.; Oyanagi, H. *Science* **1992**, *258*, 1335. (f) Riggs, P. J.; Mei, R. J.; Yocum, C. F.; Penner-Hahn, J. E.; *J. Am. Chem. Soc*. **1992**, *114*, 10650.

(11) (a) Brudvig, G. W. *Advanced EPR: Applications in Biology and Biochemistry*; Hoff, A. J., Ed.; Elsevier: Amsterdam, 1989; p 839. (b) Dismukes, G. C.; Siderer, Y. *Proc. Natl. Acad. Sci. U.S.A*. **1981**, *78*, 274. (c) Rutherford, A. W.; Boussac, A.; Zimmermann, J.-L. *New J. Chem*. **1991**, *15*, 491.

(12) (a) Cooper, S. R.; Dismukes, G. C.; Klein, M. P.; Calvin, M. *J. Am. Chem. Soc*. **1978**, *100*, 7248. (b) Cooper, S. R.; Calvin, M. *J. Am. Chem. Soc*. **1977**, *99*, 6623.

(13) (a) Renger, G. *Chem. Scr*. **1988**, *28A*, 105. (b) Kambara, T.; Govindjee *Proc. Natl. Acad. Sci. U.S.A*. **1985**, *82*, 6119. (c) Brudvig, G. W.; Crabtree, R. H. *Proc. Natl. Acad. Sci. U.S.A*. **1986**, *83*, 4586. (d) Vincent, J. B.; Christou, G. *Inorg. Chim. Acta* **1987**, *136*, L41. (e) Messinger, J.; Badger, M.; Wydrynski, T. *Proc. Natl. Acad. Sci. U.S.A*. **1995**, *92*, 3209.

(14) (a) Proserpio, D. M.; Hoffmann, R.; Dismukes, G. C. *J. Am. Chem. Soc*. **1992**, *114*, 4374. (b) Proserpio, D. M.; Rappe, A. K.; Gorun, S. M. *Inorg. Chim. Acta* **1993**, *213*, 319. (c) Yoshizawa, K.; Yamabe, T.; Hoffmann, R. *New J. Chem*. **1997**, *21*, 151. (d) Yoshizawa, K.; Ohta, T.; Yamabe, T.; Hoffmann, R. *J. Am. Chem. Soc*. **1997**, *119*, 12311. (e) Yoshizawa, K.; Hoffmann, R. *Inorg. Chem*. **1996**, *35*, 2409.

(15) Nishida, Y. *Inorg. Chim. Acta* **1988**, *152*, 73.

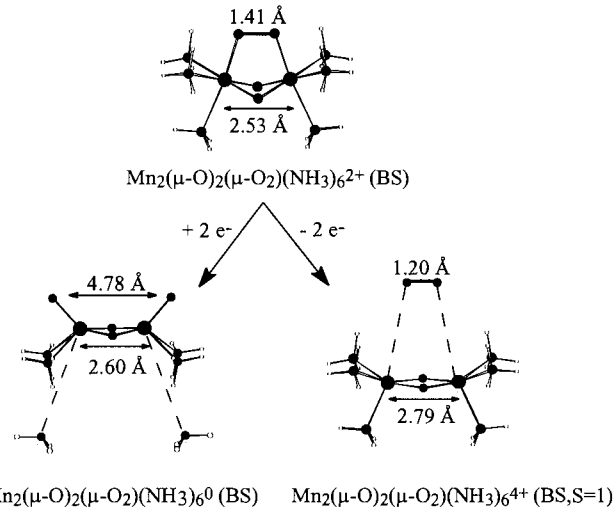

Figure 2. Optimized structures of the ground states of $Mn_2(\mu\text{-}O)_2(\mu\text{-}O_2)(NH_3)_6^{z+}$, $z = 2, 0, 4$.

dase,[18] as well as the OEC.[19] In this paper, we use approximate density functional theory to identify the key structural and electronic factors which link redox processes at a metal cluster to the formation and cleavage of bonds between atoms in the first coordination sphere. As a first step we consider the μ-peroxo species $Mn_2(\mu\text{-}O)_2(\mu\text{-}O_2)(NH_3)_6^{2+}$ (See Figure 2a) which corresponds to the intermediate stage of H_2O oxidation shown in Scheme 1. A closely related complex $Mn_2(\mu\text{-}O)_2(\mu\text{-}O_2)(Me_3TACN)_2^{2+}$,[20] has been structurally characterized by Wieghardt and co-workers[21] and shown to eliminate oxygen in aqueous solution, but the complex mixture of products obtained has made it difficult to identify the reaction pathway. In the context of the current work, the extensive structural and magnetic data available for the model complex make the μ-peroxo species a logical reference point. The electronic structure of the parent Me_3TACN complex (which differs from our chosen model only in the presence of alkyl substituents on the terminal ligands) has been described in detail in a recent paper,[22] and consequently we report only those features which are critical to the subsequent discussion of the redox processes. We have previously examined the structural consequences of one- and two-electron reduction of $Mn_2(\mu\text{-}O)_2(NH_3)_8^{4+}$,[23] where the metal core is isovalent with $Mn_2(\mu\text{-}O)_2(\mu\text{-}O_2)(NH_3)_6^{2+}$ ($Mn_2^{IV/IV}$), and the discussion of the μ-peroxo species and its redox derivatives represents a logical extension to that work. The most significant difference between the two systems is that in the μ-peroxo complex redox processes are not restricted to the metal-based manifold, but may also involve the π^* and σ^* orbitals of the O_2 unit.

Methodology

All calculations described in this paper are based on approximate density functional theory, which has been used with great success to probe structure, energetics and mechanisms in numerous transition metal-based systems.[24] Calculations were performed using the Amsterdam Density Functional (ADF), program Version 2.3,[25] developed by Baerends and co-workers. A double-ζ Slater-type basis set, extended with a single polarization function, was used to describe the hydrogen, nitrogen and oxygen atoms, while the manganese atoms were modeled with a triple-ζ basis set. Electrons in orbitals up to and including 1s {N,O} and 3p {Mn} were considered to be part of the core and treated in accordance with the frozen core approximation. A major goal of this work is to investigate the influence of the metal−metal interactions on the redox processes, and consequently we consider separately the cases where the electron spins on the two manganese centers are aligned parallel (ferromagnetic coupling) and antiparallel (antiferromagnetic coupling). The antiferromagnetically coupled states were modeled[26] using the broken-symmetry methodology developed by Noodleman et. al.,[27] which has been extensively used to describe the structural and magnetic properties of weakly coupled polymetallic systems.[28] Broken-symmetry calculations were performed by removing all symmetry elements connecting the two metal centers (giving C_s point symmetry) and imposing an asymmetry in the starting spin density. For the corresponding ferromagnetic states, where the electrons are completely delocalized, the full molecular symmetry, C_{2v}, was used. The local density approximation was employed in all cases,[29] along with the local exchange-correlation potential of Vosko, Wilk, and Nusair[30] and gradient corrections to exchange (Becke)[31] and correlation (Perdew).[32] All structures were optimized using the gradient algorithm of Versluis and Ziegler,[33] with the restriction that N−H bonds and H−N−Mn angles were constrained to 1.01 Å and 109.5°, respectively.

Results

Geometry and Electronic Structure of $Mn_2(\mu\text{-}O)_2(\mu\text{-}O_2)(NH_3)_6^{2+}$. The optimized structure of the broken-symmetry state

(16) (a) Siegbahn, P. E. M.; Crabtree, R. H. *J. Am. Chem. Soc*. **1997**, *119*, 3103. (b) Yoshizawa, K.; Yokomichi, Y.; Shiota, Y.; Ohta, T.; Yamabe, T. *Chem. Lett*. **1997**, 587. (c) Brunold, T. C.; Tamura, N.; Kitajima, N.; Moro-oka, Y.; Solomon, E. I. *J. Am. Chem. Soc.* **1998**, *120*, 5674.
(17) (a) Stavrev, K. K.; Zerner, M. C. *Theor. Chem. Acc*. **1997**, *96*, 141. (b) Stavrev, K. K.; Zerner, M. C. *Chem. Eur. J*. **1996**, *2*, 83. (c) Deng, H.; Hoffmann, R. *Angew. Chem., Int. Ed. Engl*. **1993**, *32*, 1062. (d) Dance, I. *Aust. J. Chem*. **1994**, *47*, 979. (e) Dance, I. *J. Chem. Soc., Chem. Commun*. **1997**, 165. (f) Neyman, K. M.; Nasluzov, V. A.; Hahn, J.; Landis, C. R.; Rösch, N. *Organometallics* **1997**, *16*, 995.
(18) (a) Voityuk, A. A.; Albert, K.; Köstlmeier, S.; Nasluzov, V. A.; Neyman, K. M.; Hof, P.; Huber, R.; Ramao, M. J.; Rösch, N. *J. Am. Chem. Soc*. **1997**, *119*, 3159. (b) Bray, M. R.; Deeth, R. J. *J. Chem. Soc., Dalton Trans*. **1997**, 4005.
(19) (a) Blomberg, M. R. A.; Siegbahn, P. E. M.; Styring, S.; Babcock, G. T.; Åkermark, B.; Korall, P. *J. Am. Chem. Soc*. **1997**, *119*, 8285. (b) Schmitt, E. A.; Noodleman, L.; Baerends, E. J.; Hendrickson, D. N. *J. Am. Chem. Soc*. **1992**, *114*, 6109.
(20) Me_3TACN = 1,4,7-trimethyl-1,4,7-triazacyclononane.
(21) Bossek, U.; Weyhermüller, T.; Wieghardt, K.; Nuber, B.; Weiss, J. *J. Am. Chem. Soc.* **1990**, *112*, 6387.
(22) Zhao, X. G.; Richardson, W. H.; Chen, J.-L.; Li, J.; Noodleman, L.; Tsai, H.-L.; Hendrickson, D. N. *Inorg. Chem*. **1997**, *36*, 1198.
(23) McGrady, J. E.; Stranger, R. *J. Am. Chem. Soc*. **1997**, *119*, 8512.
(24) Ziegler, T. *Chem. Rev*. **1991**, *91*, 651.
(25) *ADF 2.3.0*; Theoretical Chemistry, Vrije Univeriteit: Amsterdam. (a) Baerends, E. J.; Ellis, D. E.; Ros, P. *Chem. Phys*. **1973**, *2*, 42. (b) te Velde, G.; Baerends, E. J. *J. Comput. Phys*. **1992**, *99*, 84.
(26) The broken symmetry state is not a pure antiferromagnetic spin singlet state, but contains a weighted average of the $M_s = 0$ components of all spin states. In a number of related metal dimers we have used approximate spin projection techniques to estimate the energy of the true ground-state singlet, and in all cases found it to lie close to that of the broken-symmetry state. We are therefore confident that the general features of the potential energy surface for the broken-symmetry state are a good approximation to those of the true antiferromagnetic S = 0 state.
(27) (a) Noodleman, L.; Norman, J. G. Jr. *J. Chem. Phys*. **1979**, *70*, 4903. (b) Noodleman, L. *J. Chem. Phys.* **1981**, *74*, 5737. (c) Noodleman, L.; Case, D. A. *Adv. Inorg. Chem*. **1992**, *38*, 423.
(28) (a) Brown, C. A.; Remar, G. J.; Musselman, R. L.; Solomon, E. I. *Inorg. Chem*. **1995**, *34*, 688. (b) Ross, P. K.; Solomon, E. I. *J. Am. Chem. Soc*. **1991**, *113*, 3246. (c) Jacobsen, H.; Kraatz, H.-B.; Ziegler, T.; Boorman, P. M. *J. Am. Chem. Soc*. **1992**, *114*, 7851. (d) Bencini, A.; Gatteschi, D. *J. Am. Chem. Soc*. **1986**, *108*, 5763. (e) Andzelm, J.; Wimmer, E. *J. Chem. Phys*. **1992**, *96*, 1280. (f) McGrady, J. E.; Stranger, R.; Lovell, T. *J. Phys. Chem. A* **1997**, *101*, 6265. (g) McGrady, J. E.; Lovell, T.; Stranger, R. *Inorg. Chem*. **1997**, *36*, 3242. (h) Lovell, T.; McGrady, J. E.; Stranger, R.; Macgregor, S. A. *Inorg. Chem*. **1996**, *35*, 3079. (i) Edgecombe, K. E.; Becke, A. D. *Chem. Phys. Lett.* **1995**, *244*, 427. (j) Baykara, N. A.; McMaster, B. N.; Salahub, D. R. *Mol. Phys*. **1984**, *52*, 891.
(29) Parr, R. G.; Yang, W. *Density Functional Theory of Atoms and Molecules*; Oxford University Press: New York, 1989.
(30) Vosko, S. H.; Wilk, L.; Nusair, M. *Can. J. Phys*. **1980**, *58*, 1200.
(31) Becke, A. D. *Phys. Rev. A* **1988**, *38*, 3098.
(32) Perdew, J. P. *Phys. Rev. B* **1986**, *33*, 8822.
(33) Versluis, L.; Ziegler, T. *J. Chem. Phys*. **1988**, *88*, 322.

Table 1. Optimized Structural Parameters, Net Charges (Q), and Spin Densities (S) for Various States of $Mn_2(\mu\text{-}O)_2(\mu\text{-}O_2)(NH_3)_6^{z+}$, $z = 2, 0, 4$

	$Mn_2(\mu\text{-}O)_2(\mu\text{-}O_2)(NH_3)_6^{2+}$			$Mn_2(\mu\text{-}O)_2(\mu\text{-}O_2)(NH_3)_6^{0}$			$Mn_2(\mu\text{-}O)_2(\mu\text{-}O_2)(NH_3)_6^{4+}$		
	BS	$S = 3$	expt.[21]	BS	$S = 2$	$S = 3$	BS	BS, $S = 1$	$S = 2$
spin-α configuration	$a'^{25}a''^{17}$	$a_1^{15}a_2^{8}$ $b_1^{10}b_2^{12}$		$a'^{26}a''^{17}$	$a_1^{15}a_2^{8}$ $b_1^{10}b_2^{12}$	$a_1^{15}a_2^{8}$ $b_1^{10}b_2^{13}$	$a'^{25}a''^{16}$	$a'^{25}a''^{17}$	$a_1^{15}a_2^{7}$ $b_1^{10}b_2^{11}$
spin-β configuration	$a'^{25}a''^{17}$	$a_1^{13}a_2^{7}$ $b_1^{9}b_2^{10}$		$a'^{26}a''^{17}$	$a_1^{14}a_2^{7}$ $b_1^{9}b_2^{11}$	$a_1^{13}a_2^{7}$ $b_1^{9}b_2^{11}$	$a'^{25}a''^{16}$	$a'^{24}a''^{16}$	$a_1^{13}a_2^{7}$ $b_1^{9}b_2^{10}$
Mn−Mn/Å	2.53	2.60	2.531(7)	2.60	2.38	2.69	2.76	2.79	2.76
O−O/Å	1.41	1.40	1.46(3)	4.78	4.26	5.12	1.27	1.20	1.20
Mn−(μ-O_2)/Å	1.85	1.89	1.83(2)	1.65	1.65	1.66	2.00	4.08[a]	4.08[a]
Mn−(μ-O)/Å	1.83	1.84	1.81(2)	1.83	1.83	1.85	1.84	1.83	1.84
Mn−N_{ax}/Å	2.18	2.17	2.11[a]	4.71	4.80	4.71	2.11	2.08	2.06
Mn−N_{eq}/Å	2.19	2.17	2.11[a]	2.34	2.34	2.34	2.18	2.17	2.17
Q (Mn)	+1.14	+1.14		+1.28	+1.23	+1.30	+1.21	+1.17 +1.16	+1.16
S (Mn)	±2.55	+2.64		±2.51	+1.67	+2.68	±2.58	+3.14 −2.78	+2.94
Q (μ-O_2)	−0.39	−0.36		−0.77	−0.75	−0.77	−0.07	+0.15 +0.15	+0.13
S (μ-O)	±0.00	+0.20		±0.20	+0.28	+0.24	±0.01	+0.84 +0.85	−0.87
energy/eV	−145.48	−145.34		−159.93	−159.44	−159.75	−110.48	−111.20[a]	−110.87[a]

[a] No minimum located; parameters correspond to a fixed separation of 4.0 Å between the centers of the O−O and Mn−Mn vectors (see text).

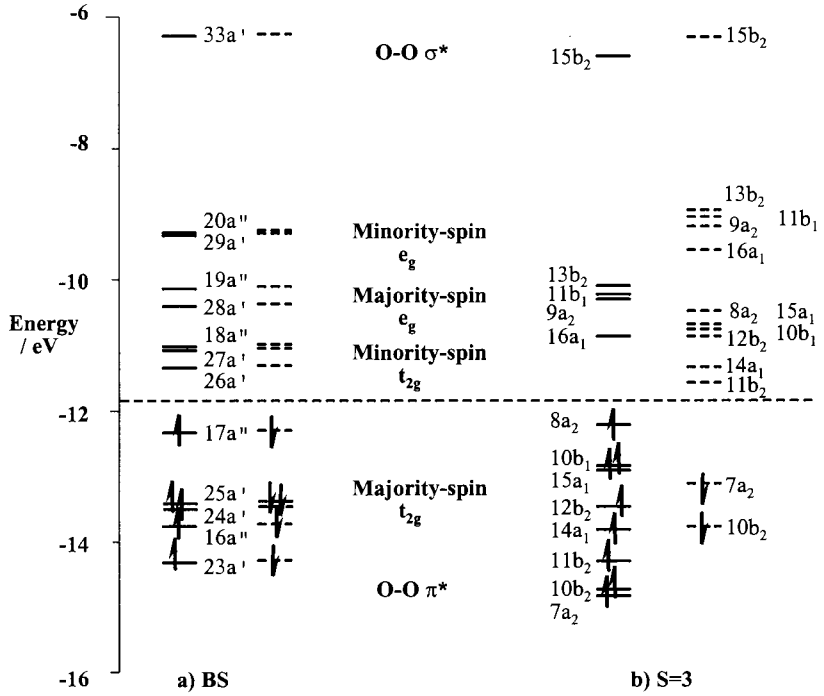

Figure 3. Molecular orbitals diagrams for the broken-symmetry and ferromagnetic ($S = 3$) states of $Mn_2(\mu\text{-}O)_2(\mu\text{-}O_2)(NH_3)_6^{2+}$.

of $Mn_2(\mu\text{-}O)_2(\mu\text{-}O_2)(NH_3)_6^{2+}$ is illustrated in Figure 2a. A full listing of the electronic configurations, energies, and optimized structural parameters for this and other species discussed in this paper is given in Table 1. The corresponding crystallographic data[21] for $Mn_2(\mu\text{-}O)_2(\mu\text{-}O_2)(Me_3TACN)_2^{2+}$ are also shown in Table 1 for comparison. The structure of the $Mn_2(\mu\text{-}O)_2(\mu\text{-}O_2)$ core is well reproduced by the calculations, with rMn−Mn (2.53 Å), rMn−(μ-O) (1.83 Å), and rMn−(μ-O_2) (1.85 Å) separations within 0.02 Å of the experimental values in each case. The O−O separation in the μ-peroxo unit (1.41 Å) is somewhat shorter than the experimental value of 1.46(3) Å, but given the large standard deviations associated with the latter, the calculated value is not unreasonable. The energies of metal- and peroxide-based orbitals are shown in Figure 3a, and are qualitatively very similar to those of the isovalent complex $Mn_2(\mu\text{-}O)_2(NH_3)_8^{4+}$ described in a previous publication.[23] The occupied majority-spin t_{2g} orbitals (24a′, 25a′, and 17a″) lie approximately 2.3 eV below their vacant minority-spin counterparts (26a′, 27a′, and 18a″), with majority- (28a′, 19a″) and minority-spin (29a′, 20a″) e_g orbitals a further 1.0 and 1.8 eV higher, respectively. The spin-α and spin-β components of each orbital are degenerate and are substantially localized on one metal center or other. The frontier orbitals of the μ-peroxo ligand span the metal manifold, with the vacant O−O σ^* orbital (33a′) almost 6 eV above the highest metal-based orbitals and the occupied π^* orbitals (16a″ and 23a′) located below the majority-spin t_{2g} subset. The out-of-plane O_2 π^* orbital overlaps in a π- fashion with metal d_{xz} (t_{2g}), and the energetic proximity of the majority-spin t_{2g} and O_2 π^* orbitals causes significant mixing of the two. The distinction between metal-based and ligand-based orbitals of a″ symmetry is therefore less clear-cut than in orbitals of a′ symmetry (17a″ has 51% O_2 π^* character, 16a″ 20%). Mulliken charges (Q) and net spin densities (S) for the two manganese centers and the atoms of the μ-peroxo bridge are also sum-

marized in Table 1. The net spin densities of ±2.55 for the manganese centers are typical of weakly antiferromagnetically coupled Mn^{IV} ions,[23] the reduction from the theoretical limit of ± 3.0 for a d^3 single ion being caused by the covalent delocalization of spin density onto the NH_3 ligands. In contrast to the substantial localization of electrons on the metal centers, the strong O−O σ bond equalizes the net spin densities on the atoms of the μ-peroxo bridge.

The ferromagnetically coupled state can be constructed from its broken-symmetry counterpart simply by inverting the electron spins on one Mn^{IV} center so that all metal-based electrons are aligned parallel, giving a resultant total spin $S = 3$. Other than a marginal increase in Mn−Mn separation (2.60 Å), optimized structural parameters for the $S = 3$ state are very similar to those of broken-symmetry ground state (Table 1), suggesting that the metal ions interact only weakly. Consistent with this, the separation between the broken-symmetry and $S = 3$ states is 0.14 eV, corresponding to an exchange coupling constant of -125 cm^{-1}.[34] This value compares favorably with the experimental estimate of -120 cm^{-1} [21] and also the value of -232 cm^{-1} reported by Noodleman et al.[22,35] The molecular orbital array for the $S = 3$ state (Figure 3b) shows qualitatively similar features to that for the broken-symmetry state, except now all the occupied majority-spin t_{2g} orbitals ($11b_2\alpha$-$8a_2\alpha$) are spin-α, and lie below their vacant minority-spin counterparts ($11b_2\beta$-$8a_2\beta$). The metal manifold is again spanned by the occupied π^* ($7a_2$, $11b_2$) and vacant σ^* ($15b_2$) orbitals of the μ-peroxo unit, but the splitting of spin-α and spin-β components of these orbitals is less marked, again due to the presence of an O−O σ bond.

Modeling of Redox Processes. For the purposes of the following discussion, we divide each redox process into two distinct steps. The first step, the vertical ionization energy, involves the transfer of two electrons to or from the parent $Mn_2(\mu\text{-}O)_2(\mu\text{-}O_2)(NH_3)_6^{2+}$ system (either in the broken-symmetry or $S = 3$ states), without any structural relaxation. In the second step, the intermediate state is allowed to relax to the optimum geometry appropriate for the redox-altered product. The purpose of separating the electron transfer process in this way is that we can associate each step with a different feature of the reaction. In principle, the relative energies of the fully optimized structures of the two oxidation states define the position of the equilibrium between the two, but it is important to realize that the computational experiment refers to isolated gas-phase species, and so neglects differential solvation of the different oxidation states. Furthermore, the energetic reference point is that of a free electron, whereas the relevant reference point in a real chemical process is the potential of the external oxidizing or reducing agent which makes up the other half of the couple. In view of these comments, it is clear that the relative energies of the optimized states do not yield useful information concerning the energetics of the reaction. Of greater significance are the relative energies of the intermediate and the fully optimized state, as these provide a measure of the driving force for internal electron transfer, once initial oxidation or reduction has occurred. By emphasizing energy differences *within* one oxidation state, rather than differences *between* oxidation states, we reduce the significance of variables such as differential solvation and instead focus on the electronic structure of the complex itself. In the following section, we will analyze the two-step redox process in detail for one example (the reduction of the broken-symmetry state of $Mn_2(\mu\text{-}O)_2(\mu\text{-}O_2)(NH_3)_6^{2+}$) by examining the electronic structure of the intermediate, and then the changes in energy and electron distribution as the cluster relaxes to its equilibrium structure. For the other redox processes, we use only the energies of the intermediate and optimized states to define the stationary points of the reaction profile.

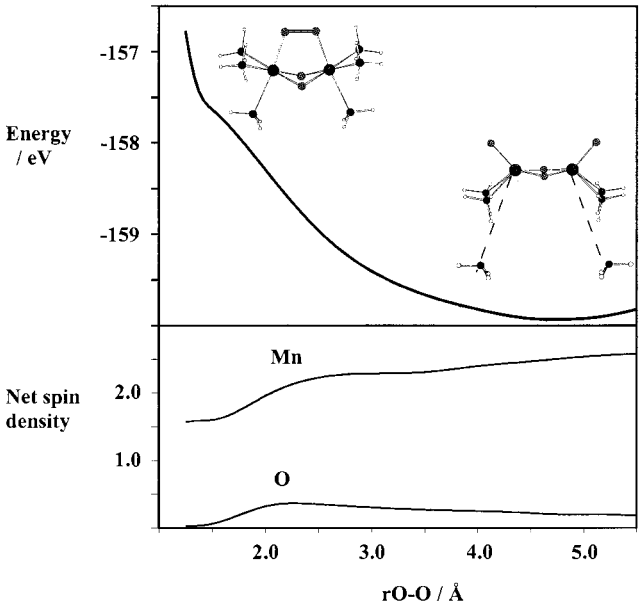

Figure 4. Variations in total energy and net spin densities during the cleavage of the O−O bond in $Mn_2(\mu\text{-}O)_2(\mu\text{-}O_2)(NH_3)_6^0$.

Two-Electron Reduction of $Mn_2(\mu\text{-}O)_2(\mu\text{-}O_2)(NH_3)_6^{2+}$. Broken-Symmetry State. The addition of two electrons to the broken-symmetry state of $Mn_2(\mu\text{-}O)_2(\mu\text{-}O_2)(NH_3)_6^{2+}$ populates the two lowest unoccupied spin−orbitals, 26a′α and 26a′β (Figure 3a), which form part of the minority-spin t_{2g} manifold. Net spin densities decrease from ±2.55 to ±1.63 electrons per metal center, consistent with the formation of two Mn^{III} ions in an intermediate $S = 1$ spin state. The energy changes associated with the subsequent geometry relaxation step are shown as a function of the separation of the oxygen atoms in the μ-peroxo unit in Figure 4. All other parameters, with the exception of N−H distances and H−N−Mn angles, were allowed to optimize freely. In the optimized structure (Figure 2b), rO−O = 4.78 Å, rMn−(μ-O_2)[36] = 1.65 Å, and rMn−N_{ax} = 4.71 Å (compared to values of 1.41, 1.85, and 2.18 Å respectively for the parent peroxo complex). Thus reduction brings about the complete cleavage of the O−O bond, along with the dissociation of the NH_3 groups lying trans to the μ-peroxo unit, resulting in approximate square-pyramidal coordination about the manganese centers. In contrast, the central $Mn_2(\mu\text{-}O)_2$ core remains largely unperturbed (rMn−Mn increases by only 0.07 Å along the reaction coordinate). The electronic origin of these changes can be traced by monitoring the spin densities at the manganese and oxygen centers (of the μ-peroxo unit) along the reaction coordinate (Figure 4). As the O−O separation is increased, the electrons in the σ bond begin to localize at opposite ends of the μ-peroxo unit, increasing the net spin densities at the oxygen atoms to a maximum value of ±0.32 at rO−O ≈ 2.2 Å. After this point, the developing spin density at the oxygen centers is

(34) The exchange coupling constant, J, was calculated using $H = -2JS_1 \cdot S_2$ and the formula $E(S_{max}) - E(BS) = -JS^2_{max}$.[27]

(35) The difference between the value reported here and the estimate given in ref 22 probably arises because in the current study the energy of the $S = 3$ state corresponds to that of the fully optimized structure.

(36) For simplicity, we retain the (μ-O_2) label to identify the oxygen atoms derived from the peroxo group of the parent complex, despite the fact that cleavage of the O−O bond effectively eliminates the bridge. This formalism is also applied to the oxidation processes, where the O_2 unit dissociates.

Scheme 2. Electron Transfer Pathways for Two-Electron Reduction of $Mn_2(\mu\text{-}O)_2(\mu\text{-}O_2)(NH_3)_6^{2+}$

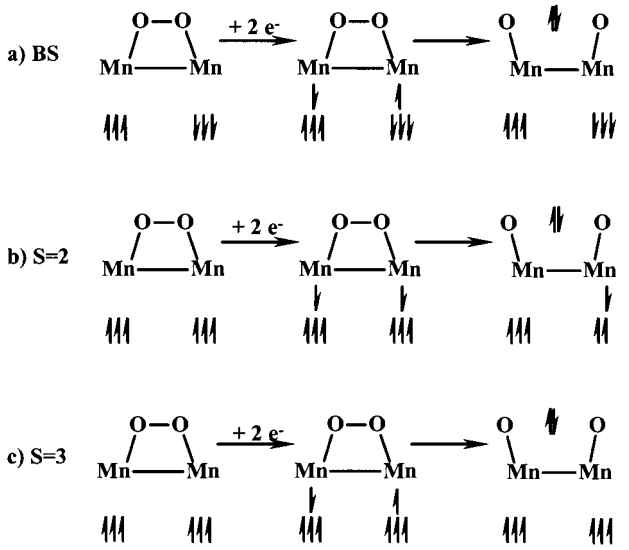

countered by the transfer of an electron, of opposite spin, from the minority-spin t_{2g} orbitals of the Mn^{III} ions into the O−O σ^* orbital. Net spin densities at each oxygen center therefore decrease to a limiting value of ± 0.20, while those at the metal center increase from ± 1.63 to ± 2.51, close to the original value of ± 2.55 characteristic of a Mn^{IV} ion in its $S = {}^3/_2$ ground state. The internal electron-transfer pathway, from initial metal based reduction through to population of the O−O σ^* orbital, is summarized in Scheme 2a.

In the optimized structure, the μ-peroxo ligand has been replaced by two Mn^{IV}═O groups, accounting for the contraction of the Mn−O distance, and it is the strong trans influence of the oxo ligands which causes the dissociation of the axial NH_3 ligands noted previously (rMn−N = 4.71 Å). The rates of heterolytic O−O bond cleavage reactions have been extensively studied, and they are accelerated by electron donating ligands in the trans position (the so-called "push-effect").[37] This is apparently contrary to our observation of complete dissociation of the trans ligand. However, in the present case the bond cleavage occurs only after reduction of the metal centers, and so stabilization of a high-valent metal-oxo species is not necessary. These observations suggest an important role for the protein environment in supplying labile donor residues capable of reversible coordination in response to changes in electronic structure at the active site.

The potential energy curve in Figure 4 shows that, following initial electron transfer to the metal centers, O−O bond cleavage is highly exothermic, the optimized structure (rO−O = 4.78 Å) lying over 2.5 eV below the intermediate state (1.41 Å). The driving force for the internal electron transfer is provided by a combination of two factors, the formation of two strong Mn═O double bonds and the regeneration of the stable half-filled t_{2g}^3 subshell of Mn^{IV}. In contrast, cleavage of the O−O bond at the $Mn_2(\mu\text{-}O)_2(\mu\text{-}O_2)(NH_3)_6^{2+}$ oxidation level can occur only at the expense of removing two electrons from the stable majority-spin t_{2g} orbitals (Figure 3a), and is consequently endothermic by approximately 2.4 eV. It should be noted that the additional stability of the half-filled t_{2g}^3 subshell only emerges from a spin-unrestricted treatment of the electronic structure, and similar conclusions would therefore not necessarily arise from studies using extended Hückel theory. It is

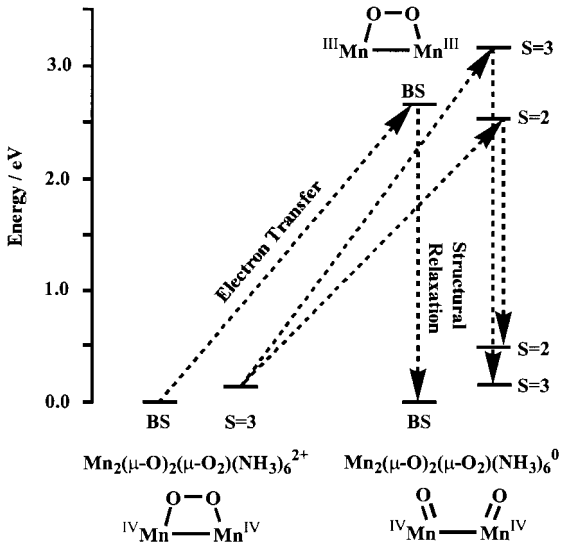

Figure 5. Energy profiles for the two-electron reduction of $Mn_2(\mu\text{-}O)_2(\mu\text{-}O_2)(NH_3)_6^{2+}$ to $Mn_2(\mu\text{-}O)_2(\mu\text{-}O_2)(NH_3)_6^{0}$. For each oxidation state, the energy of the ground state is taken as an arbitrary zero point. Absolute energy differences *between* oxidation states are not relevant, because gas-phase values neglect differences in solvation energy (see text for full discussion of this point).

also instructive at this point to compare our results with a recent publication by Bérces,[38] describing dioxygen complexes of a copper dimer, where it was concluded that the spin-restricted theory was sufficient for an accurate description of the O−O bond cleavage process. This may simply be a result of the lower spin polarization in Cu^{2+} (d^9, $S = {}^1/_2$) relative to Mn^{4+} (d^3, $S = {}^3/_2$). Alternatively, it may be significant that in the copper species, cleavage of the O−O bond occurs along an axis orthogonal to, rather than parallel to, the metal−metal vector, making stabilization of the developing spin density in the breaking bond by the metal centers impossible.

Ferromagnetically Coupled State ($S = 3$). The molecular orbital array for the $S = 3$ state of $Mn_2(\mu\text{-}O)_2(\mu\text{-}O_2)(NH_3)_6^{2+}$ (Figure 3b) indicates that the two lowest-lying unoccupied spin− orbitals are again part of the minority-spin t_{2g} manifold. In this case, however, they are of the same spin ($11b_2\beta$ and $14a_1\beta$), with the lowest-lying spin-α orbitals (majority-spin e_g) some 0.5 eV higher in energy, and so initial two-electron reduction gives an intermediate $Mn_2^{III/III}$ state with total spin $S = 2$. Relaxation of the geometry again results in cleavage of the O−O bond (rO−O = 4.26 Å, Table 1), but in this case the driving force for internal electron transfer is 0.5 eV lower than for the corresponding broken-symmetry state (Figure 5). The internal electron transfer is again driven by two factors, the formation of two Mn═O bonds and the regeneration of the $Mn_2^{IV/IV}$ core. The stablising influence of the Mn═O bonds is essentially independent of the orientations of the electron spins, but the stability of the $Mn_2^{IV/IV}$ core is not (Scheme 2b). To cleave the O−O bond, the σ^* orbital must be occupied by two electrons of opposite spin, whereas in the intermediate $Mn_2^{III/III}$ state with $S = 2$, the two highest-energy electrons occupy orbitals of the same spin (β). The spin-α electron required to populate the O−O σ^* orbital must therefore be taken from a more stable majority-spin t_{2g} orbital, with the net result that, in the optimized dioxo structure, one of the two Mn^{IV} ions is in an excited spin-doublet state (average spin density = +1.67).

If instead the two additional electrons are forced to occupy orbitals of the same spatial and spin symmetry as O−O σ^* ($b_2\alpha$,

(37) Dawson, J. H. *Science* **1988**, *240*, 433.

(38) Bérces, A. *Inorg. Chem.* **1997**, *36*, 4831.

$b_2\beta$, total spin $S = 3$), O−O bond cleavage occurs to give a dioxo complex 0.31 eV more stable than the $S = 2$ state, and only 0.18 eV higher than the broken-symmetry ground state. Structural parameters for the broken-symmetry and $S = 3$ states of $Mn_2(\mu\text{-}O)_2(\mu\text{-}O_2)(NH_3)_6^0$ are very similar, just as they were for the corresponding spin states of $Mn_2(\mu\text{-}O)_2(\mu\text{-}O_2)(NH_3)_6^{2+}$, consistent with the fact that at both oxidation levels, the two are simply related by an inversion of the spins at one Mn^{IV} center. While the structures and relative energies of the fully optimized broken-symmetry and $S = 3$ states are relatively insensitive to the nature of the coupling between the metal ions, the same is not true of the $Mn_2^{III/III}$ intermediates, where the $S = 3$ state lies approximately 0.4 eV higher. In the broken-symmetry state, the excess electrons in the $Mn_2^{III/III}$ intermediates occupy two minority-spin t_{2g} orbitals, whereas in $S = 3$, one electron is placed in the $13b_2\alpha$ orbital, part of the much higher-energy majority-spin e_g manifold. In single-ion terms, the $Mn_2^{III/III}$ intermediate with $S = 3$ contains one Mn^{III} center in an $S = 1$ state and one in an $S = 2$ state (Scheme 2c). As a result, it is substantially less stable than the corresponding broken-symmetry and $S = 2$ states, where both ions are in the more stable $S = 1$ state. This final point serves to illustrate that while it is computationally expedient, when metal centers are weakly coupled, to calculate the ferromagnetically coupled ground-state rather than its antiferromagnetic counterpart,[16a] this procedure should be viewed with some caution when examining reaction pathways.

The ideas presented in the preceding paragraphs can be summarized as follows: in both antiferromagnetically and ferromagnetically coupled systems, initial two-electron reduction of $Mn_2(\mu\text{-}O)_2(\mu\text{-}O_2)(NH_3)_6^{2+}$ is metal-based, resulting in the formation of a μ-peroxo $Mn_2^{III/III}$ intermediate. Subsequent cleavage of the O−O bond then occurs by transfer of two electrons, necessarily of *opposite spin*, from the metal manifold into O−O σ^*, thereby regenerating the stable $Mn_2^{IV/IV}$ core. If the metal core is antiferromagnetically coupled, the lowest energy $Mn_2^{III/III}$ intermediate has two electrons in high-lying metal-based orbitals of the same spatial and spin symmetry as the O−O σ^* orbital (Scheme 2a), providing a low-energy electron-transfer pathway linking the antiferromagnetically coupled ground states of $Mn_2(\mu\text{-}O)_2(\mu\text{-}O_2)(NH_3)_6^{2+}$ and $Mn_2(\mu\text{-}O)_2(\mu\text{-}O_2)(NH_3)_6^0$. In contrast, the most stable $Mn_2^{III/III}$ intermediate arising from reduction of a ferromagnetically coupled core ($S = 2$) has two high-energy electrons in orbitals of the same spin, in which case cleavage of the O−O bond can occur only at the expense of removal of an electron from the more stable majority-spin t_{2g} orbitals (Scheme 2b). The alternative intermediate $Mn_2^{III/III}$ complex, where electrons are in appropriate spatial and spin symmetry for transfer into the O−O σ^* orbital, is relatively unstable due to the presence of a high-spin Mn^{III} ion (Scheme 2c). Thus we conclude that the barrier to O−O bond cleavage is much higher when the metal centers are ferromagnetically coupled.

Two-Electron Oxidation of $Mn_2(\mu\text{-}O)_2(\mu\text{-}O_2)(NH_3)_6^{2+}$. Broken-Symmetry State. The energy profile for the two-electron oxidation of the broken-symmetry state of $Mn_2(\mu\text{-}O)_2(\mu\text{-}O_2)(NH_3)_6^{2+}$ is shown in Figure 6, and the electron-transfer pathway is summarized in Scheme 3a. Initial oxidation removes electrons from the $17a''\alpha$ and $17a''\beta$ orbitals (Figure 3a), giving rise to a $Mn_2^{V/V}$ intermediate with two vacancies of opposite spin in the majority-spin t_{2g} manifold. The $17a''$ orbitals are extensively delocalized over both metal centers and the μ-peroxo ligand, and so the initial electron transfer step is not as strongly localized on the metal ions as the reduction processes described above. Nevertheless, the geometry relaxation step does result in transfer of charge from ligand to metal, albeit to a smaller extent than in the reduction processes, and so the qualitative conclusions based on the assumption of an initial metal-based oxidation process remain valid. Following formation of this $Mn_2^{V/V}$ intermediate, there are two possible pathways for internal electron transfer from ligand to metal, both of which are shown in Scheme 3a. Pathway (i) involves transfer of two electrons *of opposite spin* from one component of the π^* orbital of O_2 unit into the vacancies in the majority-spin t_{2g} manifold, thereby

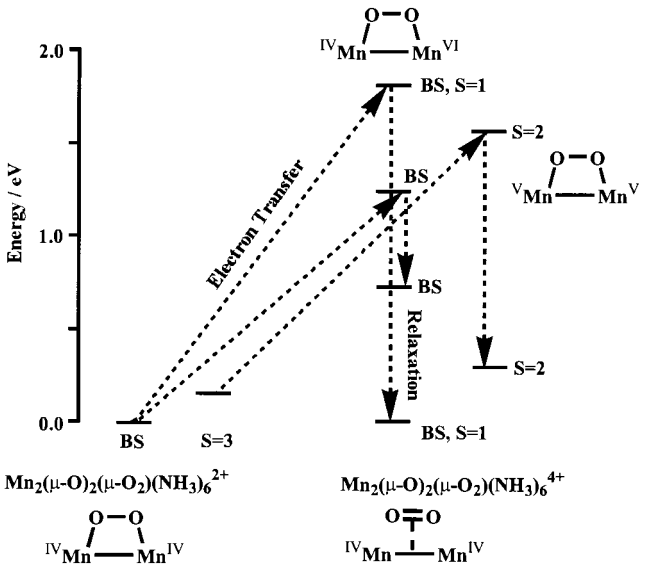

Figure 6. Energy profiles for the two-electron oxidation of $Mn_2(\mu\text{-}O)_2(\mu\text{-}O_2)(NH_3)_6^{2+}$ to $Mn_2(\mu\text{-}O)_2(\mu\text{-}O_2)(NH_3)_6^{4+}$.

Scheme 3. Electron Transfer Pathways for Two-Electron Oxidation of $Mn_2(\mu\text{-}O)_2(\mu\text{-}O_2)(NH_3)_6^{2+}$

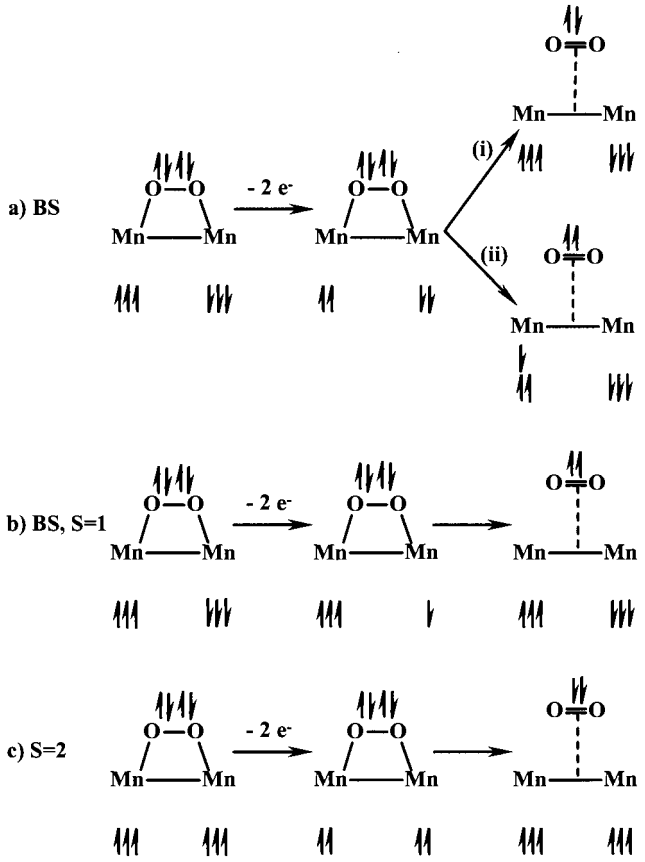

regenerating the $Mn_2^{IV/IV}$ core in its broken-symmetry ground state, but producing O_2 in an excited spin singlet state. Pathway (ii) involves transfer of two electrons *of the same spin*, one from each component of O_2 π^*, generating oxygen in a triplet state, but the $Mn_2^{IV/IV}$ core in an excited state with one electron in a minority-spin t_{2g} orbital. In the optimized structure, the net spin densities of ± 0.01 and ± 2.58 for O and Mn, respectively (Table 1) indicate that of the two possibilities, (i) is more stable, and the structural parameters, rO−O = 1.27 Å, rMn−(μ-O_2) = 2.00 Å, are consistent with the formulation of the product as a molecule of oxygen, in its spin-singlet excited state, weakly coordinated to the manganese dimer. In terms of the functionality of the OEC, the production of O_2 in a spin singlet state presents a problem, because the additional energy required for the spin interconversion to a triplet ($\sim$1 eV)[2d] presents a significant barrier.

As an alternative strategy, the oxidation process could remove two electrons from orbitals of the same spin and spatial symmetry as the orthogonal components of the π^* orbital of O_2 ($a'\beta$, $a''\beta$), giving a spin-triplet. This state is denoted BS, $S = 1$, to emphasize that despite its nonzero total spin, it is derived from the broken-symmetry, rather than ferromagnetically coupled, parent complex. Relaxation of the geometry again causes an increase in the Mn−(μ-O_2) bond length, but in this case to a much greater extent. No minimum in the potential energy surface was located for rMn−(μ-O_2) < 4.0 Å, beyond which point convergence problems occur due to the near degeneracy of the O_2 π^* and minority-spin t_{2g} orbitals. However, at rMn−(μ-O_2) = 4.0 Å the energy of the cluster is lower than the sum of the energies of the isolated O_2 and $Mn_2(\mu\text{-}O)_2(NH_3)_6^{4+}$ fragments, indicating that a minimum, corresponding to a weakly bonded O_2 complex, is present at some longer separation. In keeping with the weak nature of the interaction, the potential energy surface is very flat at large rMn(μ-O_2), and so the energy and structural parameters of the complex at rMn−(μ-O_2) $\approx$ 4.0 Å will closely approximate those of the true minimum. Accordingly, the data reported in Table 1 correspond to a fixed distance of 4.0 Å between the centers of the Mn−Mn and O−O vectors. The very long Mn−(μ-O_2) and short O−O bonds confirm that the O_2 molecule is bound to the metal centers only by weak noncovalent forces, and the net spin densities of +0.85 per oxygen center confirm that the oxygen molecule is in its spin-triplet ground state, stabilizing the BS, $S = 1$ state by 0.72 eV relative to the corresponding state containing spin-singlet oxygen. However, the corresponding intermediate state, is relatively unstable (Figure 6), because the removal of two electrons *of the same spin* from an antiferromagnetically coupled system generates one Mn^{IV} ion and one Mn^{VI} (Scheme 3b) rather than a symmetric $Mn_2^{V/V}$ species (Scheme 3a). Therefore while an antiferromagnetically coupled core provides a low energy pathway for reductive cleavage of the O−O σ bond, oxidative formation of the π bond passes through a high-energy intermediate.

Ferromagnetic Coupled State ($S = 3$). Oxidation of the ferromagnetically coupled ($S = 3$) state of $Mn_2(\mu\text{-}O)_2(\mu\text{-}O_2)(NH_3)_6^{2+}$ results in the removal of two electrons of the same spin from the majority-spin t_{2g} manifold, giving a state with $S = 2$. The molecular orbital diagram shown in Figure 3b indicates that the occupied majority-spin t_{2g} manifold is a relatively narrow band of six orbitals, and consequently the initial electron transfer step can generate fifteen distinct configurations, all with $S = 2$, and all of similar energy. Of these, we focus only on the configuration where electrons are removed from $8a_2\beta$ and $12b_2\beta$ (the same symmetry as the two components of the O−O π^* orbital) in which case subsequent internal electron transfer can generate both metal and O_2 units in their respective ground states. This intermediate lies approximately 0.4 eV above the lowest-lying of the fifteen configurations (corresponding to removal of electrons from $8a_2\beta$ and $10b_1\beta$). However, we noted in the Introduction that metal ions in vivo are typically in asymmetric environments, in which case symmetry-imposed barriers vanish. The energy of the intermediate described here can therefore be regarded as an upper limit for a system of lower molecular symmetry. It is important to emphasize again the difference between arguments based on spatial symmetry, which are dependent on coordination environment, and those based on spin symmetry, which are not. Relaxation of the $S = 2$ state again results in a contraction of the O−O vector and a substantial lengthening of the Mn−(μ-O_2) bonds, but attempts to locate a minimum in the potential energy surface are again frustrated by convergence problems at large rMn−(μ-O_2). Therefore the energies and structural parameters reported for the $S = 2$ state in Table 1 again correspond to a fixed separation of 4.0 Å between the centers of the Mn−Mn and O−O vectors. In the optimized structure, the net spin density of −0.87 per oxygen center indicate that the weakly bound oxygen molecule is its ground state, as are both Mn^{IV} centers (S(Mn) = +2.94), and so the $S = 2$ state is related to the BS, $S = 1$ state described earlier simply by a spin flip at one Mn^{IV} center. The distinction between the BS, $S = 1$ and $S = 2$ electron transfer pathways emerges in the stability of the intermediate states, which for the former, contained a relatively high energy $Mn_2^{IV/VI}$ core (Scheme 3b). Scheme 3c illustrates that in contrast, removal of the two electrons of the same spin from the ferromagnetically coupled system generates a more stable $Mn_2^{V/V}$ intermediate. Thus oxidative formation of the π component of the O−O bond proceeds via a lower-energy pathway in the presence of ferromagnetically coupled metal centers.

Summary

The calculations described in this paper reveal a number of features of the electronic structure of manganese clusters that may be relevant to the functionality of the OEC and other redox metalloenzymes. The stability of the half-filled t_{2g}^3 subshell makes Mn^{IV} ions unusually resistant to both reduction and oxidation, so much so that the $Mn_2^{IV/IV}$ core persists across all three oxidation states, $Mn_2(\mu\text{-}O)_2(\mu\text{-}O_2)(NH_3)_6^{4+/2+/0}$. In this context, it is interesting to speculate that the prevalence of Mn^{IV} (d^3), Mn^{II} (d^5), and Fe^{III} (d^5) centers in electron-transfer enzymes[1] is related to the stability of the half-filled shells. The second notable feature is the role of metal−metal interactions in determining the barriers to formation of the O−O σ and π bonds. The major differences between the antiferromagnetically coupled and ferromagnetically coupled systems arise from the need to link bond formation or cleavage between ligand atoms to an external electron source (or sink) via a low-energy electron-transfer pathway. Cleavage (or the microscopic reverse, formation) of the O−O σ bond requires transfer of two electrons of opposite spin between metal and ligand, while formation (or cleavage) of the O−O π bond requires transfer of two electrons of the same spin. Two-electron reduction or oxidation of $Mn_2(\mu\text{-}O)_2(\mu\text{-}O_2)(NH_3)_6^{2+}$ provides the necessary electrons or oxidizing equivalents in high-lying minority-spin or low-lying majority-spin t_{2g} orbitals, respectively. If the metal ions are antiferromagnetically coupled, then the additional electrons (or vacancies) occupy orbitals of opposite spin, whereas ferromagnetic coupling directs the electrons into orbitals of the same spin. Thus at an antiferromagnetically coupled core, reductive

cleavage of the O−O σ bond occurs via a relatively stable $Mn_2^{III/III}$ intermediate containing two low-spin Mn^{III} ions (Figure 5, Scheme 2a), but oxidative formation of the O−O π bond must pass through a high-energy $Mn_2^{IV/VI}$ intermediate (Figure 6 and Scheme 3b). In contrast, reductive cleavage of the O−O σ bond at a ferromagnetically coupled site occurs via an unstable $Mn_2^{III/III}$ intermediate containing a high-spin Mn^{III} ion, whereas oxidative formation of the π bond involves a relatively stable $Mn_2^{V/V}$ intermediate (Figure 6 and Scheme 3c).

In terms of the reactivity of the OEC, the antiferromagnetic coupling induced by the $Mn_2(\mu\text{-}O)_2$ core provides an ideal electronic environment for formation of the σ component of the O−O bond, but not for the π component. Shaik and coworkers[39] have recently noted the importance of two-state reactivity in the context of oxidation of organic substrates, and it is possible that the barrier to oxidative formation of the π bond could be reduced by initial formation of the more stable antiferromagnetically coupled (BS) intermediate, followed by spin interconversion to the BS, $S = 1$ potential surface at a later point along the reaction coordinate (Figure 6). Alternatively, the reaction could involve initial population of the ferromagnetic $S = 3$ state of $Mn_2(\mu\text{-}O)_2(\mu\text{-}O_2)(NH_3)_6^{2+}$, from which point the low-energy $S = 2$ pathway can be accessed. Noodleman has previously suggested that thermal population of the $S = 3$ state of $Mn_2(\mu\text{-}O)_2(\mu\text{-}O_2)(Me_3TACN)_6^{2+}$ may provide a pathway for oxygen dissociation,[22] in general agreement with our results, although we have shown that release of the O_2 group only occurs following two-electron oxidation. The ferromagnetic pathway could be made more accessible by structural modifications that reduce the exchange coupling constant, for example, protonation of the μ-oxo groups.[40] It seems unlikely, however, that protonation of the bridges would follow oxidation, which reduces the basicity of the oxo ligands. A rather more subtle possibility is suggested by the structure of the OEC (Figure 1), where the Mn−Mn separations of 2.7 Å (typical of a $Mn_2(\mu\text{-}O)_2$ unit) and 3.3 Å (typical of $Mn_2(\mu\text{-}O)$) indicate the presence of two very different electronic environments. Magnetic coupling in mono-μ-oxo bridged complexes is typically an order of magnitude weaker than in di-μ-oxo bridged systems,[2] making ferromagnetic states more accessible if the peroxo ligand bridges the former rather than the latter. The presence of four, rather than two, manganese centers in the OEC may therefore be related to the need to provide different electronic environments for the sequential formation of the σ and π components of the O−O bond.

We stated in the Introduction that our aim was to investigate the "chemical competence" of species which may play a role in the reaction cycle, and it is therefore important to critically assess the key intermediates we propose in light of available experimental evidence. There is a considerable body of data to support the participation of metal oxo species, such as those in $Mn_2(\mu\text{-}O)_2(\mu\text{-}O_2)(NH_3)_6^0$, in the initial stage of the oxidative process. Vibrational spectra have been reported for Mn^{IV}═O complexes,[41a] along with UV/vis and mass spectra suggesting the existence of a $(Mn^{IV}═O)_2$ dimer.[41b] Stable Mn^V═O complexes are also well established in the literature,[42] and Mn^V intermediates have been implicated in the catalytic oxidation of water[2d,13d,e] and various organic substrates.[43] Analogous Fe^{IV}═O species also play a prominent role in a number of well-characterized enzymes, containing both heme (cytochrome P450, horseradish peroxidase)[44a,b] and non-heme (methane monoxygenase, ribonucleotide reductase) active sites.[44c−f] As noted in the Introduction, the participation of a μ-peroxo intermediate in the OEC has been questioned,[13e] but such species are well established in the literature,[2b−c,45,46] and have been postulated as intermediates in synthetic water oxidation catalysts.[43c] Moreover, their importance in the microscopic reverse, oxygen activation, has been established by vibrational spectroscopy, notably in methane monoxygenase.[8,44d−h] Finally, although there is no direct experimental evidence concerning the site of O_2 release in the OEC, a number of bimetallic complexes are capable of reversibly binding molecular oxygen in its triplet ground state, and, significantly, the majority have metal−metal separations in excess of 3.0 Å.[46] As a result, ferromagnetic states will be accessible at room temperature, giving access to low-energy electron-transfer pathways for reductive cleavage of the π component of the O−O bond.

Acknowledgment. We acknowledge the support of The University of York Innovation and Research Priming Fund and the Australian Research Council. We also acknowledge the helpful comments of a referee regarding the nature of the weak interaction between oxygen and the tetravalent cluster.

IC981253K

(39) Shaik, S.; Filatov, M.; Schroder, D.; Schwarz, H. *Chem. Eur. J.* **1998**, *4*, 193.

(40) (a) Baldwin, M. J.; Stemmler, T. L.; Riggs-Gelasco, P. J.; Kirk, M. L.; Penner-Hahn, J. E.; Pecoraro, V. L. *J. Am. Chem. Soc.* **1994**, *116*, 11349. (b) Larson, E. J.; Riggs, P. J.; Penner-Hahn, J. E.; Pecoraro, V. L. *J. Chem. Soc., Chem. Commun.* **1992**, 102. (c) Wieghardt, K.; Bossek, U.; Nuber, B.; Weiss, J.; Bonvoisin, J.; Corbella, M.; Vitols, S. E.; Girerd, J. J. *J. Am. Chem. Soc.* **1988**, *110*, 7398. (d) Hagen, K. S.; Westmoreland, T. D.; Scott, M. J.; Armstrong, W. H. *J. Am. Chem. Soc.* **1989**, *111*, 1907.

(41) (a) Czernuszewicz, R. S.; Su, Y. O.; Stern, M. K.; Macor, K. A.; Kim, D.; Groves, J. T.; Spiro, T. G. *J. Am. Chem. Soc.* **1988**, *110*, 4158. (b) Sakiyama, H.; Okawa, H.; Isobe, R. *J. Chem. Soc., Chem. Commun.* **1993**, 882. (c) Ayougou, K.; Bill, E.; Charnock, J. M.; Garner, C. D.; Mandon, D.; Trautwein, A. X.; Weiss, R.; Winkler, H. *Angew. Chem., Int. Ed. Engl.* **1995**, *34*, 343.

(42) (a) Collins, T. J.; Powell, R. D.; Slebodnik, C.; Uffelman, E. S. *J. Am. Chem. Soc.* **1990**, *112*, 899. (b) Collins, T. J.; Gordon-Wylie, S. W. *J. Am. Chem. Soc.* **1989**, *111*, 4511.

(43) (a) Holm, R. H. *Chem. Rev.* **1987**, *87*, 1401 (b) Srinivasan, K.; Michaud, P.; Kochi, J. K. *J. Am. Chem. Soc.* **1986**, *108*, 2309. (c) Naruta, Y.; Sasayama, M.; Sasaki, T. *Angew. Chem., Int. Ed. Engl.* **1994**, *33*, 1839.

(44) (a) Sono, M.; Roach, M. P.; Coulter, E. D.; Dawson, J. H. *Chem. Rev.* **1996**, *96*, 2841. (b) Penner-Hahn, J. E.; Smith Eble, K.; McMurry, T. J.; Renner, M.; Balch, A. L.; Groves, J. T.; Dawson, J. H.; Hodgson, K. O. *J. Am. Chem. Soc.* **1986**, *108*, 7819. (c) Dong, Y.; Yan, S.; Young, V. G., Jr.; Que, L. Jr. *Angew. Chem., Int. Ed. Engl.* **1996**, *35*, 618. (d) Que, L., Jr. Dong, Y. *Acc. Chem. Res.* **1996**, *29*, 190. (e) Que, L., Jr. *J. Chem. Soc., Dalton Trans.* **1997**, 3933. (f) Liu, K. E.; Valentine, A. M.; Wang, D.; Huynh, B. H.; Edmondson, D. E.; Salifoglou, A.; Lippard, S. J. *J. Am. Chem. Soc.* **1995**, *117*, 10174. (g) Liu, K. E.; Wang, D.; Huynh, B. H.; Edmondson, D. E.; Salifoglou, A.; Lippard, S. J. *J. Am. Chem. Soc.* **1994**, *116*, 7465. (h) Liu, K. E.; Valentine, A. M.; Qiu, D.; Edmondson, D. E.; Appelman, E. H.; Spiro, T. G.; Lippard, S. J. *J. Am. Chem. Soc.* **1995**, *117*, 4997.

(45) (a) Kitayama, N.; Moro-oka, Y. *Chem. Rev.* **1994**, *94*, 737. (b) Niederhoffer, E. C.; Timmons, J. H.; Martell, A. E. *Chem. Rev.* **1984**, *84*, 137.

(46) (a) Menage, S.; Brennan, B. A.; Juarez-Garcia, C.; Münck, E.; Que, L., Jr. *J. Am. Chem. Soc.* **1990**, *112*, 6423. (b) Dong, Y.; Menage, S.; Brennan, B. A.; Elgren, T. E.; Jang, H. G.; Pearce, L. L.; Que, L., Jr. *J. Am. Chem. Soc.* **1993**, *115*, 1851. (c) Kayatani, T.; Hayashi, Y.; Suzuki, M.; Uehara, A. *Bull. Chem. Soc. Jpn.* **1994**, *67*, 2980. (d) Hayashi, Y.; Suzuki, M.; Uehara, A.; Mizutani, Y.; Kitagawa, T. *Chem. Lett.* **1992**, *91*. (e) Hayashi, Y.; Kayatani, T.; Sugimoto, H.; Suzuki, M.; Inomata, K.; Uehara, A.; Mizutani, Y.; Kitagawa, T.; Maeda, Y. *J. Am. Chem. Soc.* **1995**, *117*, 11221. (f) Ookubo, T.; Sugimoto, H.; Nagayama, T.; Masuda, H.; Sato, T.; Tanaka, K.; Maeda, Y.; Okawa, H.; Hayashi, Y.; Uehara, A.; Suzuki, M. *J. Am. Chem. Soc.* **1996**, *118*, 701.